University of Northern Iowa

UNI ScholarWorks

2017

Magnetic behavior of bulk and nanostructured MnxTaS2

Lucas Paul Beving
University of Northern Iowa

Recommended Citation

MAGNETIC BEHAVIOR OF BULK AND NANOSTRUCTURED Mn$_x$TaS$_2$

A Thesis Submitted
in Partial Fulfillment
of the Requirements for the Designation
University Honors

Lucas Paul Beving
University of Northern Iowa
May 2017

This Study by:

Entitled:

has been approved as meeting the thesis requirement for the Designation University Honors

_____
Date   Dr. Paul Shand, Honors Thesis Advisor, Physics Department

_____
Date   Dr. Jessica Moon, Director, University Honors Program

Introduction

At its base, material science research aims to categorize specific materials by their various attributes, such as structure, integrity, electronic properties, magnetic properties, and others. By categorizing materials in this way, it becomes easier to generalize the application of a specific material to those within a broader category. The interest in materials that exhibit useful characteristics at small scales derives directly from the technology industry's need for smaller and smaller devices. Two-dimensional materials are of great interest for this reason.

Two-dimensional materials are comprised of many single layers, or planes, stacked together to create a crystal. Each layer may be composed of single or multiple elements. The layers interact weakly with one another; consequently, the properties of the material may be largely determined by the characteristics of the layers. The electronic properties of these materials were researched in detail within the last decades. The result of this research was the categorization of specific two-dimensional materials as insulators, semimetals, superconductors, metals, and semiconductors (Ajayn, Kim, & Banerjee, 2016). Two-dimensional materials that are chemically similar to any of the specific materials exhibiting these properties quickly become candidates for similar behavior. The research that produced the results detailed within this work was completed with the above results in mind.

The material described in this work is composed of layers of tantalum sulfide between which manganese was deposited. The number of manganese atoms per one tantalum is called the concentration, x. In contrast to the research that led to the categorizations described above, the magnetic properties of this material were explored.

Specifically, this project aimed to characterize the magnetic phase transitions of bulk and nanostructured samples of manganese intercalated tantalum disulfide (Mn_xTaS_2) using several

well documented analysis methods such as those used by Anthony Arrott and John Noakes

(Arrott & Noakes, 1967). Determining and comparing these magnetic characteristics will

provide both novel results and a basis for subsequent projects.

Background

In order to understand the significance of this study the following information must be

understood: the structure of the material and the basic properties of different kinds of magnetism.

The basic structure of the material being used throughout this project is shown on the left

side of Figure 1. The entire structure, crystalline or nanostructured, is formed from this basic

structure; one layer of manganese seated, or intercalated, between layers of tantalum disulfide.

The manganese atoms control the magnetic properties of the entire material. The amount of

manganese within these layers also determines the exact type of magnetism that the material will
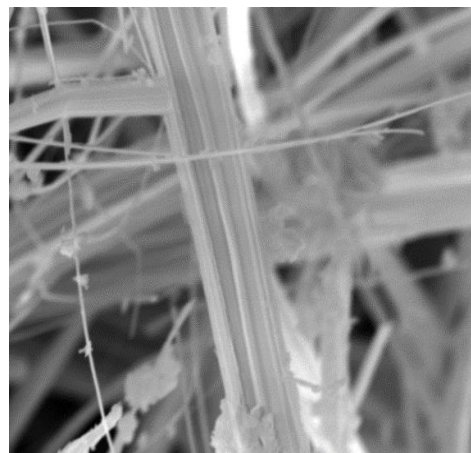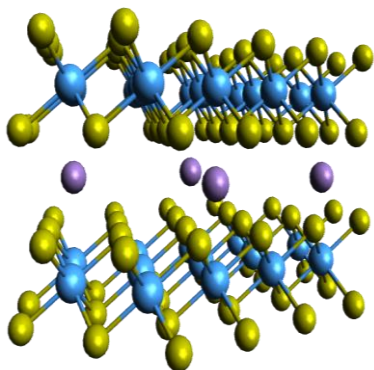
demonstrate.

Figure 1.

Left: The crystal structure of Mn_xTS_2: Yellow=Sulfur, Blue=Tantalum, Purple=Manganese.
Image created using Avogadro by Mathew Fleming, Physics Dept. University of Northern Iowa.

Right: A picture of a sample taken with a scanning electron microscope. Taken by Payton
Burken, Physics Dept. University of Northern Iowa.

When the basic structure on the left side of Figure 1 is extended horizontally and repeated vertically, the structure produced is called crystalline. Alternatively, wrapping this basic structure around in the shape of a cylinder forms a nanotube—the fundamental building block of nanostructured samples. An example of the nanostructured material is shown on the right side of Figure 1.

Within this work, magnetization and magnetic susceptibility will be mentioned continually. First, the magnetization of a particular sample is the total magnetic moment produced by the sample. This is calculated by adding together the strength of each of the atomic magnetic moments (due to the manganese) comprising the sample. These magnetic moments are physical-constructs related to the size of the magnetic field produced by the magnetic atoms. The magnetic field produced by a single atom is comparable to that of a bar magnet in structure, only on the atomic scale. Secondly, the magnetic susceptibility is a measure of the response of a material to an applied magnetic field. Mathematically, one would write $\mathcal{X} = M/H$, where $\mathcal{X}$ is the magnetic susceptibility, M is the magnetization and H is the applied field. Specific changes in the susceptibility as a function of temperature mark phase transitions in the material. The various magnetic phases of a material range from well-ordered ferromagnetism to disordered spin and cluster-glass phases. Finally, the magnetic phases described here will be limited to the following: ferromagnetism, antiferromagnetism, paramagnetism, and spin/cluster-glass.

Ferromagnetism is an ordered form of magnetism where the individual magnetic moments all tend to align in a single direction. In a similar manner, all of the moments comprising an antiferromagnetic material are aligned or anti-aligned with a specific direction. Each moment in such a material is anti-aligned, or pointing along the same line in the opposite direction, with each of its neighbors. In ferromagnetic materials the moments are aligned as in

the antiferromagnetic material but the strength of moments pointing in one direction are larger. In contrast to these ordered phases, in the paramagnetic phase, each moment rotates about in an unordered manner. A material in such a state would have no measurable magnetization. The types of magnetism described above are shown in Figure 2.
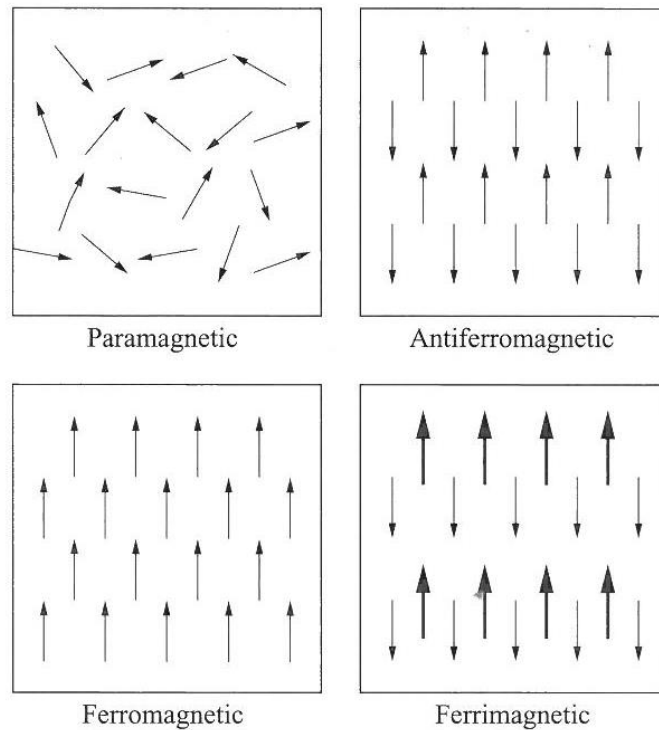

Paramagnetic   Antiferromagnetic

Ferromagnetic   Ferrimagnetic

Figure 2. Illustrations of four magnetic phases. Reprinted from *Magnetic Materials* (13), by N. Spaldin, 2003, Cambridge, UK: Cambridge University Press. Copyright [2003] by Nicola Spaldin.

Finally, it is important to note that the magnetic properties of the system depends on the concentration of manganese within the material. The concentration relative to tantalum is denoted x. This is the number of manganese atoms per single tantalum found in the material. Thus, the material is denoted as Mn_xTaS_2.

A greater understanding of the structure, magnetism, and types of magnetism will be used to provide a basis for understanding this work.

Literature Review

Transition metal dichalcogenides

Tantalum disulfide falls into the category of a low-dimensional solid. This is a result of the fact that the tantalum disulfide layers are bound together by weak forces. An entire solid crystal is composed of a large number of single layers, which by themselves are planar (two-dimensional). There are other materials that may be considered two-dimensional including graphite, mica, and many others. Tantalum disulfide is also a transition-metal dichalcogenide. This group of materials is typified by a structure where the transition metal is nested within two layers of a chalcogenide, a material partially composed of an element from group 6 of the periodic table. Molybdenum disulfide is a well know material in this category. These materials have several interesting properties. Most notably is the variance in the materials' electronic band structure for each of its polytypes (Friend & Yoffe, 1987). Each polytype references a different orientation between consecutive layers of the material. Figure 3 shows two such polytypes for molybdenum disulfide. These materials also have interesting applications, such as the use of molybdenum disulfide as a lubricant.

The transition-metal dichalcogenides also have interesting electronic properties. The electronic properties present in a specific transition metal dichalcogenide depend strongly on the
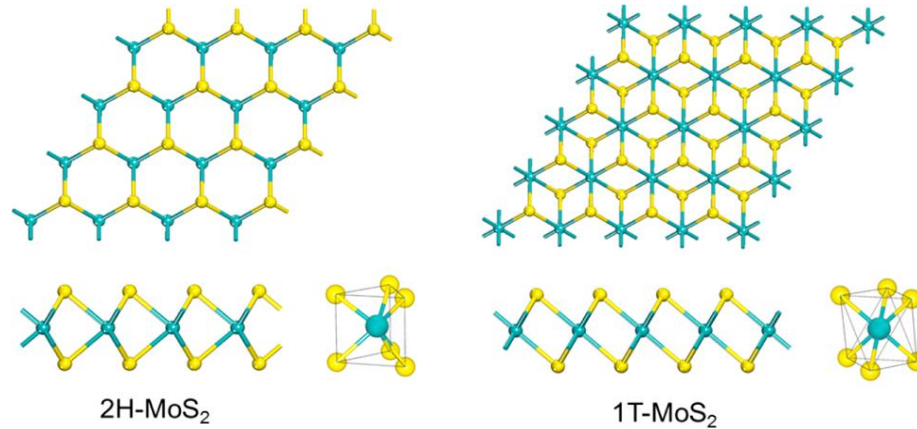
Figure 3. In the 2H polytype the chalcogenide atoms define the vertices of a triangular prism, while in the 1T polytype they define the vertices of an octahedron. Tang, et al., *Chemistry of Materials* **27**, 3743 (2015)

group from which the transition metal is taken. The Group IV dichalcogenides act as semiconductors and semimetals. The Group V dichalcogenides exhibit changes in their structure in response to periodic lattice distortion-charge density wave (PLD-CDW) transitions. The effects of these transitions depend on the polytype of the material. Of great interest is the competition between the superconducting phase and CDW in specific transition metal dichalcogenides (Friend & Yoffe, 1987). Although the transition metal dichalcogenides have interesting properties in their unaltered state, much interest lies in properties of the intercalated forms of these materials.

Magnetism

> **Magnetic Phases.** A transition metal dichalcogenide is called intercalated when foreign atoms are introduced between layers of the original material. This is shown specifically for tantalum disulfide on the left side of Figure 1. In addition, intercalating a magnetic atom such as manganese into a transition metal dichalcogenide allows the entire structure to have magnetic behavior. There are 14 basic types of magnetic order that can occur in solids (Hurd, 1982).

However, this research is only concerned with ferromagnetism, antiferromagnetism, paramagnetism, and spin/cluster-glasses.

In the paramagnetic phase, magnetic interactions between atomic moments within the material are weak in comparison with thermal effects. The moments in such a material rotate about their fixed positions is space due to random thermal activation. This disordered state occurs at temperatures higher than a critical temperature, below which an ordered state exists (Hurd, 1982).

Ferromagnetism is an ordered state of the magnetic moments of a material in which neighboring moments align with each other due to their mutual interactions. This neighbor-neighbor alignment is a long-range phenomenon that gives the material a spontaneous magnetization.

If the distance between neighboring moments is increased from the ferromagnetic state, neighboring moments will begin to become antiparallel with one another. This is the ordered state of antiferromagnetism. In this case no spontaneous magnetization should exist since each moment is nullified by its neighbor (Hurd, 1982).

Spin-glass behavior is established in a material when it is lowered to significantly low temperatures and the atomic moments are disordered, meaning the spacing between moments is not constant. The disorder allows both ferromagnetic and antiferromagnetic interactions to occur. The antiferromagnetic interactions can lead to frustration for the system. Frustration occurs when the system cannot reach its lowest energy state. This is the case when three atomic moments lie at the vertices of an equilateral triangle and interact through antiferromagnetism. Each of the moments will not be aligned antiparallel to one of its neighbors in the lowest energy state. Such frustration produces interesting behavior in the spin-glass state: the time for the

system to reach an equilibrium state is large. Cluster-glass materials act in a similar manner;

however, entire groups of atomic moments interact via ferromagnetism or antiferromagnetism

rather than single moments (Hurd, 1982).

Theories. This section will describe some of the theories used to describe the behavior

of magnetic materials near phase transitions.

In 1967 Anthony Arrott and John Noakes proposed an equation of state for nickel in the

region of its ferromagnetic phase transition (Arrott and Noakes, 1967). The equation was meant

to fit data in a more accurate that way previously taken by other researchers. The equation is

usually written in the following way:

$$\left(\frac{H}{M}\right)^{1/\gamma} = a\frac{T - T_C}{T_C} + bM^{1/\beta}$$

Here H is the applied magnetic field, M is the magnetization, T_C is the critical

temperature, and a and b are constants. Combining this equation with magnetization and field

data allows for the extraction of the exponents γ and β. This form of data analysis has recently

been used to determine magnetic phase characteristics in $La_{0.7}Ca_{0.3}Mn_{1-x}Fe_xO_3$ (Ginting et al.,

2015) and the disordered polycrystalline alloys $Cr_{75}Fe_{25}$ and $Cr_{75}Fe_{30}$ (Fisher, Kaul, &

Kronmuller, 2002). The so called critical exponents γ and β are defined in the following ways

(Stanley, 1971):

$$M \sim (-t)^\beta$$

$$\chi \sim t^{-\gamma}$$

with

$$t = \frac{T - T_C}{T_C}$$

The critical exponent gamma is defined by way of the susceptibility $X = H/M$. It is important to note that both exponents are defined in zero-applied field. There are various theoretical derivations for the values of these exponents. The Mean Field Theory gives $\gamma = 1$, $\beta = 0.5$. Renormalization-group theory for the 2-D Ising model gives $\gamma = 1.238$, $\beta = 0.326$ and the 3-D Heisenberg model gives $\gamma = 1.386$, $\beta = 0.365$ (Peles, 1991). These exponents, and others, can be related by using an assumption about the thermodynamic potentials of the system. Scaling theory assumes that the thermodynamic potentials of the system (e.g., Gibbs) are generalized homogeneous functions of their variables (Stanley, 1971). A generalized homogeneous function is one of several variables (here two) such that the following is true for arbitrary numbers a and b.

$$f(\varepsilon^a x, \varepsilon^b y) = \varepsilon f(x, y)$$

This assumption in conjunction with several calculations yields relationships between the various exponents such as the following.

$$\Delta = \gamma + \beta$$

The new exponent Δ is called the gap exponent. This relation will provide a way to check the agreement of the measured values of γ and β. The research of James Kouvel and Michael Fisher (1964) also provides another avenue to the values of γ and β. Similar to that of Arrott and Noakes (1967), the research of Kouvel and Fisher (1964) was completed using nickel. Their equations for the critical exponents are the following (Fisher, Kaul, & Kronmuller, 2002):

$$M_0 \left(\frac{dM_0}{dT}\right)^{-1} = \frac{(T - T_c)}{\beta}$$

$$X_0^{-1} \left(\frac{dX_0^{-1}}{dT}\right)^{-1} = \frac{(T - T_c)}{\gamma}$$

In these equations the 0 subscript signifies a value in zero applied field. Thus, M_0 is the

spontaneous magnetization and $\mathcal{X}_0$ is the zero-field susceptibility. This method, and those

preceding it, will be useful in characterizing the behavior of the material near the paramagnetic

to ordered-phase transition.

A separate method of analysis must be employed for the temperature regimes where the

material exhibits spin-glass behavior. The Vogel-Fulcher-Tammann (VFT) law was developed

and used over decades to describe the relaxation characteristics of glass-like magnetism

(Shtrikman & Wohlfarth, 1981). The VFT describes the relaxation time τ as an exponential

function of the difference between the current temperature T and the glass transition temperature

T_0:

$$\tau = \tau_0 e^{E_A/k_B(T-T_0)}$$

In this equation, E_A and τ_0 are constants. Using VFT for analysis requires applying AC magnetic

fields of varying frequencies to the material. The average relaxation time can then be determined

from the equation given above.

Much like VFT allows for the specific characterization of spin-glass behavior, a

hysteresis plot characterizes the ferromagnetic behavior of a material. A standard hysteresis plot

is shown in Figure 4 below. Magnetization data is taken at a single temperature for varying

applied magnetic field strengths. The arrows on the graph below illustrate how the applied field

is varied. First, the field is increased until the magnetization saturates, i.e. all the atomic

moments are aligned in one direction. As the field strength is decreased, the magnetization

decreases. This continues until the field strength reaches zero, at which point it is important to

note that the magnetization of the material is *not* zero. The value B$_r$ is called the remenance of

the sample. The field is then increased in the opposite direction until the magnetization of the

sample reaches zero. The field strength needed to accomplish this is called the coercivity, H_c. Materials with higher values of coercivity are called hard ferromagnets, while those of lower coercivity are called soft ferromagnets. The analysis of data of this form will allow for the characterization of the ferromagnetic behavior exhibited by the Mn_xTaS_2 samples.
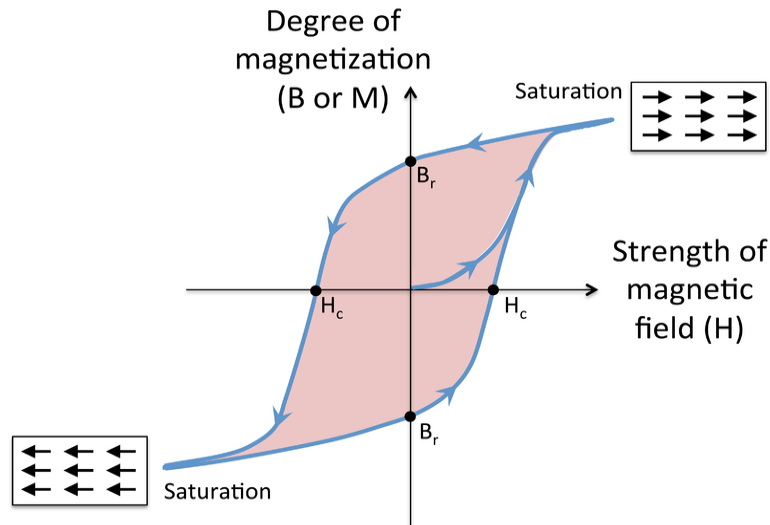

Figure 4. The standard form of a magnetic hysteresis loop. Creative Commons *Hysteresis loop for a ferromagnet* by Tem5psu is licensed under CC BY 2.0

Motivation. The motivation for this project stems primarily from recent work on magnetically intercalated 1D dichalcogenide nanostructures (Kidd et al., 2012). The nanostructured samples were fabricated from elemental powders using long heating periods. The resulting tubular structure is shown on the right side of Figure 1. The materials were seen to have spin glass behavior at low temperatures and ferromagnetic behavior below 85 Kelvin. Further motivating work includes an in-depth magnetic analysis of two specific nanostructured samples, i.e. $Mn_{0.15}TaS_2$ and $Mn_{0.23}TaS_2$ (Shand et al.,2015).

This project aims to extend the measurement and analysis techniques of these reports to samples of different concentrations. The concentrations investigated by this project would be between $x = 0.1$ and $x = 0.3$. Determining the concentration dependence of magnetic phase

transitions of manganese intercalated tantalum disulfide would then be completed as described in the following sections.

Research Questions to Be Answered. There are two questions motivated by the above review and by the researcher's interests. First, what are the magnetic properties of nanostructured manganese intercalated tantalum disulfide for various manganese concentrations? Second, how do these properties compare with those of the bulk crystalline material? Answering these questions would provide information on the possible applications of these structures and the effects of magnetic intercalation on nanostructures.

Methodology

This project was completed through the following steps: sample fabrication, manganese concentration measurement, sample loading into Physical Properties Measurement System (PPMS), magnetic measurements using the PPMS, and data analysis using several well documented methods.

The nanostructured samples were fabricated from elemental powders using long heating periods in glass ampoules. The heating process included a day at 125 °C, an increase to 700 °C, a hold at an annealing temperature, and finally a slow cooling (Kidd et al., 2012). Dr. Laura Strauss worked to create nanostructured samples of varying concentrations for this project and other related experiments.

Energy Dispersive X-Ray Spectroscopy (EDX) was performed on the samples to determine the relative concentrations of manganese, tantalum, sulfur, and impurities. These measurements were carried out by the members of Dr. Timothy Kidd's research group in the Physics Department. Such a measurement bombards the sample with electrons to produce X-rays of varying energy. The characteristic X-rays of the elements present in the material can

then be identified. The relative intensity of the X-rays gives the relative amounts of each

element. The error in such measurements is approximately ±10%.

The samples were then crushed and inserted into delrin sample holders (approximately

146 cubic millimeters). Due to the fact that a measurement of the sample's mass is more easily

made than that of its volume, subsequent susceptibility values were measured by per unit mass.

Mass measurements were taken using a Mettler AE260 Delta Range Analytic Balance Scale.

The sample holders were secured to the AC Transport module of the Quantum Design

PPMS via a clear plastic straw. The system was sealed and the desired measurement sequence

was initiated from the control panel. Depending on the type of measurement, the sample was left

within the system for 6-12 hours. The sample was then removed and placed in a desiccation

vessel for storage. Data from any measurement was then saved and converted to the necessary

format for analysis.

It is important to note that due to a lack of sample holders, samples were systematically

moved from storage vial to sample holder and back to storage vial. Thus, if more data was

required from a specific sample, then the mass associated with the new measurement would have

been different from that of the original. In general, this was avoided simply by planning the

measurements in advance; however, this was not always possible in the event of system

maintenance and data collection for other experiments.

The data analysis methods included Arrott-Noakes, Kouvel-Fisher, Vogel-Fulcher-

Tammann, and Curie-Weiss analysis. The first of these uses the Arrott-Noakes equation of state

to extract fitting parameters from computer aided data fits. These parameters, so-called critical

exponents, have allowed us to characterize the magnetic phase transitions of each sample. The

method of Kouvel and Fisher determines the same critical exponents using different equations.

Curie-Weiss analysis has been used to determine the temperature at which each samples transitions from the paramagnetic state to an ordered state. Vogel-Fulcher-Tammann analysis would have been implemented when a sample shows signs of spin or cluster-glass behavior.

These methods have been implemented using *MatLab* and *Origin 8*. These systems were chosen due to the author's familiarity with the tools and documentation of each. *MatLab* allows one to write scripts of code that the *MatLab* program then executes. Such scripts may include lengthy or repeated calculations. The results of the script can then be rendered in many graphical formats that are part of the *MatLab* package. On the other hand, *Origin 8* acts as a more scientifically sophisticated version of Microsoft Excel. Each column in a sheet can easily be manipulated mathematically and plotted. *Origin 8* can then be used to determine the curve that best fits a data set. This allows one to extract values (such as those described in the theories section) from a given data set.

After applying these methods to both the nanostructured and bulk sample, the dependence of transition temperature on concentration between the two structures have been compared.

It is important to note that the majority of the data collection and analysis was completed during the University of Northern Iowa 2015 Summer Undergraduate Research Program and the following academic year. Work on the 18% manganese nanostructured sample began on June 22nd, 2015 with a calculation of the specified concentration. Field cooled, zero-field cooled and Arrott-Noakes data for this sample was collected during the same week. The following two weeks consisted of determining the transition temperature and critical exponents from the data using the previously written *MatLab* program and relations from scaling theory. The same data as described above was collected and analyzed periodically throughout the fall semester of 2015

for the crystalline sample. This left ample time to organize and complete this work and the

presentation accompanying it during the spring semester of 2017.

Results

Since this work aims to compare the results determined from the measurement of two

samples that differ magnetically and structurally, this section shall be divided into two

subsections to detail the findings for each sample.

Nanostructured $Mn_{0.18}TaS_2$

As noted above, there were a limited number of sample holders available during the

execution of this project. In the case of the nanostructured sample, all but one of the

measurements was made with a single sample. The isothermal measurements required for

Arrott-Noakes and Kouvel-Fisher analysis techniques were conducted over several months, and

thus required the use of two samples of the 18% manganese nanostructured material. Table 1

lists the measured and calculated values for each mass.

Sample designation	Mass of filled sample holder (grams)	Mass of empty sample holder (grams)	Mass of sample (grams)
m_1	0.7388	0.3501	0.3887±0.0003
m_2	0.5339	0.3520	0.2019±0.0003

Table 1. Masses of the two samples of the nanostructured $0.18MnTaS_2$.

The mass of the two samples were determined by calculating the difference between the

mass of the full and empty sample holder. The first type of analysis done on the m_1 sample was

a Curie-Weiss analysis, which uses the following equation.

$$X_{DC} = \frac{C}{H - \theta}$$

Taking the inverse of this equation gives a linear equation with slope $1/C$ and intercept $-\theta/C$. The data was graphed and fit with a linear equation in the region where the data behaved linearly using Origin 8. The data and plot are shown in Figure 5.
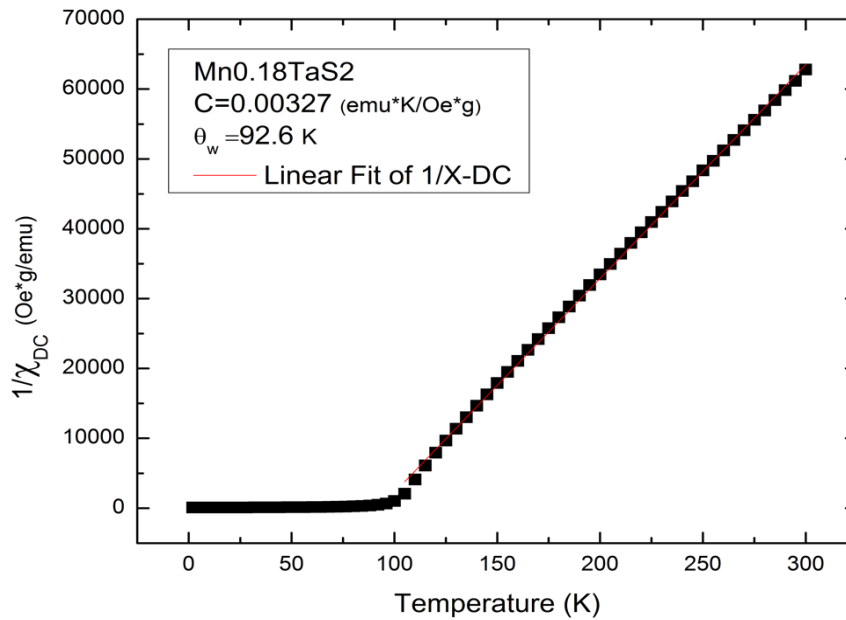

Figure 5. A plot of the inverse susceptibility for the m_1 sample. The purely paramagnetic regime begins at approximately 100 Kelvins.

From the above fit we can then estimate both θ (which represents T_c) and C. The values are given in Table 2. A reasonable interval for the paramagnetic temperature was obtained from the parameters above.

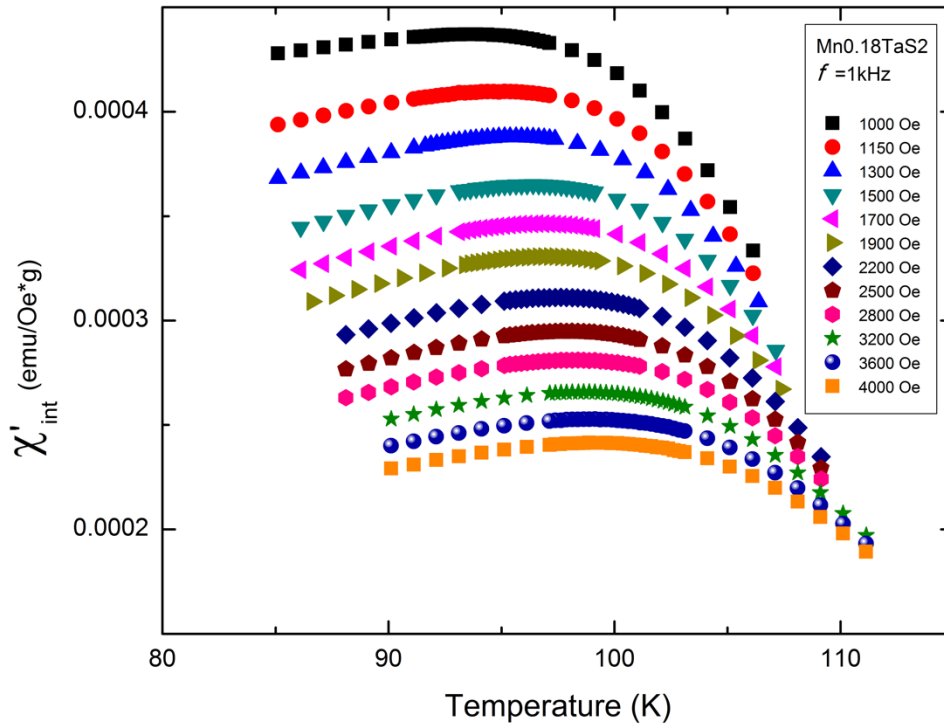| Fit Parameter	Value
θ (K)	93 ± 1
C (emu · K/Oe · g)	0.00326 ±0.00002

Table 2. Curie-Weiss parameters.

Figure 6. A plot of $\mathcal{X}'_{int}$ as a function of Temperature. The shift in the peak as the applied field increases is a signature of a PM to FM

Next, AC susceptibility data was plotted for various bias fields (Figure 6). Unlike the Curie-Weiss susceptibility, the AC susceptibility is calculated from data taken when a small oscillatory field is applied. Expanding a Maclaurin power series about this field (h) gives the magnetization as

$$M = M_0 + \mathcal{X}_1 h + \mathcal{X}_2 h^2 + \mathcal{X}_3 h^3 \dots$$

(M_0 is the spontaneous magnetization). Those susceptibilities can be expanded into the following form due to their oscillatory nature.

$$\mathcal{X}_n = \sqrt{(\mathcal{X}'_n)^2 + (\mathcal{X}''_n)^2}$$

$$\mathcal{X}'_n = \mathcal{X}\cos(\theta) \quad and \quad \mathcal{X}''_n = \mathcal{X}\sin(\theta)$$

In these expressions $\mathcal{X}$ is the magnitude of the susceptibility and θ is the phase. $\mathcal{X}'_n$ is the in-phase component of the specific non-linear susceptibility, while $\mathcal{X}''_n$ is the out-of-phase

component. Measurements can be made of both of these values for specific frequencies and

harmonics. These measurements then allow for the identification of trends characteristic of a

certain magnetic phase. For example, if the peak temperature of $\mathcal{X}'$ increases as the strength of

the applied field increases, then the current magnetic phase of the system would be

ferromagnetic. One can see this effect in Figure 6.

     As the bias field increases in strength the peak in $\mathcal{X}'_{int}$ shifts to higher temperatures.

Recall that the susceptibility is a measure of the response of the sample relative to the applied

field. It is expected that the maximum in-phase susceptibility of a substance undergoing a PM to

FM transformation will occur at higher temperatures for higher bias fields. This is because the

atomic moments align more easily in a higher field than for a lower field. The data above is

taken as a signature of a PM to FM transition.

     For certain measurements, as in Figure 6, it is imperative to know the field strength in the

interior of the sample. This is termed the internal field and is given by the following.

$$H_{int} = H - NM$$

Here, N is the demagnetizing factor, which is calculated using the magnetization data of the

sample for low applied fields at a single temperature.

     Next, the data from the same measurement as shown in Figure 6 was used to create a

scaling plot of peak susceptibility against a scaling variable involving the reduced temperature

$(\varepsilon = (T - T_c)/T_c)$ and the internal field (H_{int}) . The reduced temperature is defined using the

transition temperature (T_c). The data in Figure 7 was fitted by eye to determine the transition

temperature and critical exponent delta. Note that $\Delta = \gamma + \beta$. The collapse of data onto a

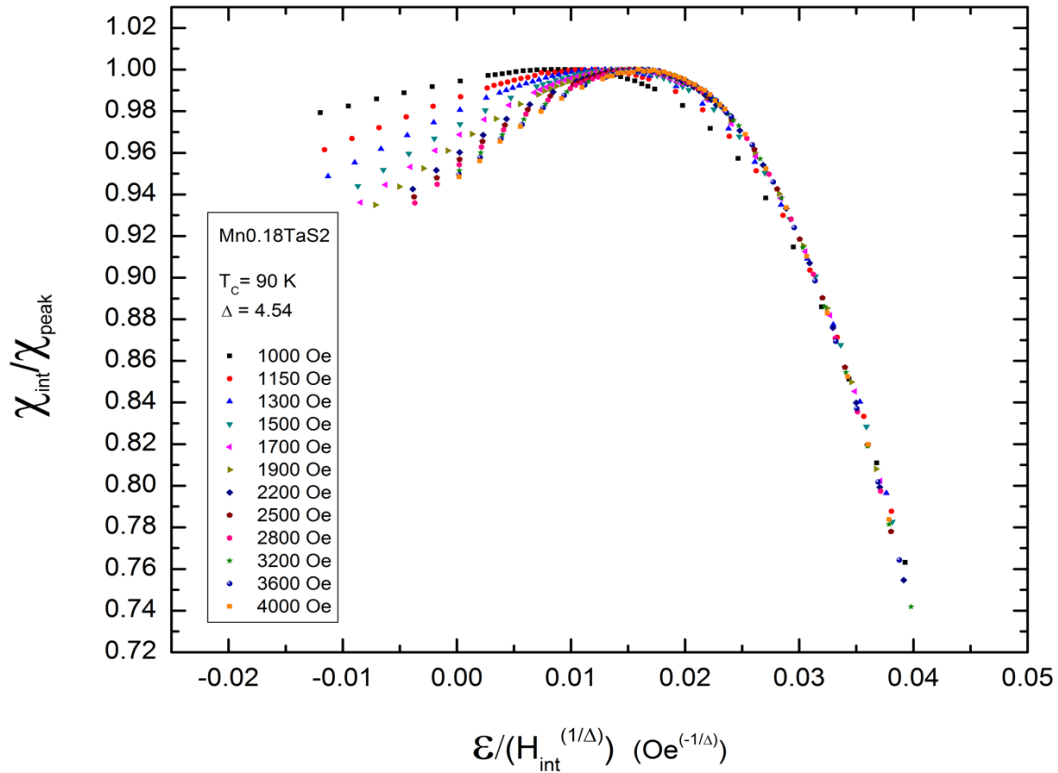universal curve is indicative of a phase transition.

Figure 7. A scaling relation plotted in Origin 8. Such a relation
utilizes critical exponents to show a universal curve or relation.

In the case of a PM to FM transition the correlation length becomes infinite as the system

becomes ordered. The susceptibility undergoes a large change as well because of the existence

of the spontaneous magnetization of the FM state. Experimentation continued on the first sample

with data taken in two forms. To take *zero-field cooled* (ZFC) data the sample temperature is

initialized at 150 °K. The sample chamber is then cooled at a constant rate of 8 °K/min to a base

temperature of 2°K in zero DC magnetic field. DC magnetization data is then taken as the

sample warms up at 5 °K/min rate in an applied DC field of 30 Oe. This data taking protocol is

accompanied by *field cooled* (FC) data. This secondary protocol takes DC magnetization data in

an applied DC field of 30 Oe as the sample cools from 150 °K to 2 °K at a rate of 8 °K/min.
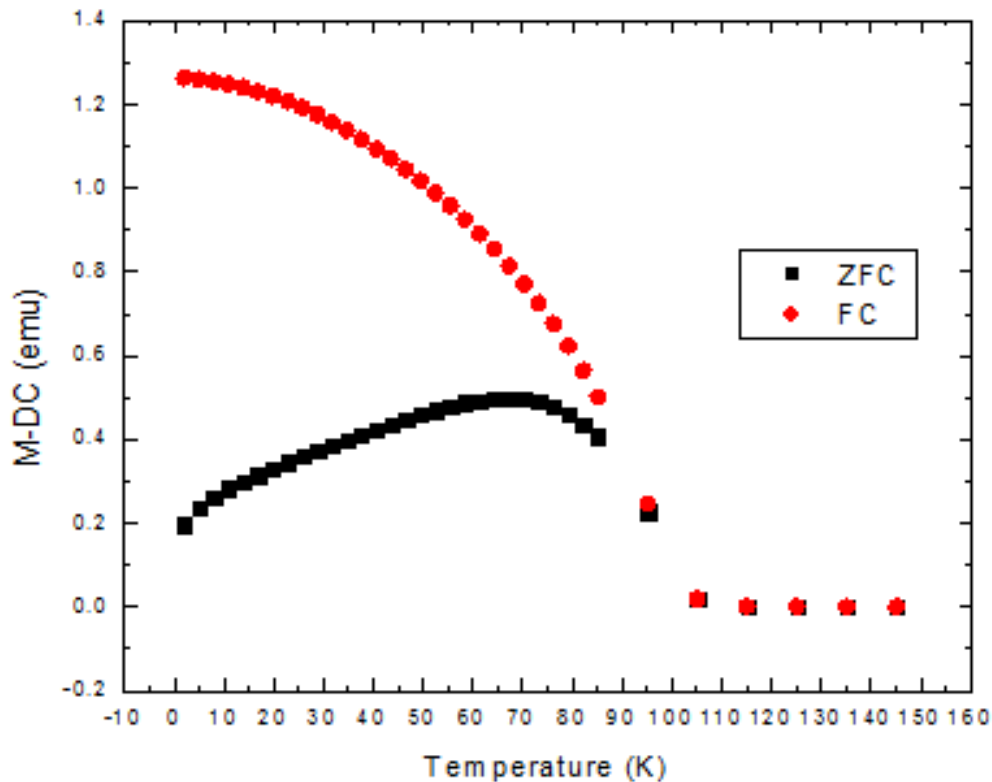
Both sets of data are shown in Figure 6.

Figure 8. Plot of ZFC and FC data. The apparent position of the bifurcation comports with the believed PM to FM transition.

A bifurcation is the signature attribute of a FC-ZFC plot. The relative position of the bifurcation in Figure 8 agrees with the previous indications of a PM to FM transition occurring around 95-105 °K. The split in data occurs at a much higher temperature than the peak in the ZFC data. If the transition were glassy the split would occur very close to the peak magnetization.

One of the final sets of data taken using the first sample was composed of two hysteresis loops. The data is in the format of magnetization vs applied field for a single temperature. Hysteresis occurs in ferromagnetic materials due to the fact that even in the absence of an applied field the material is still magnetized. An important characteristics of the hysteresis loop is the coercivity, the width of the loop. The two measurements below seem to have no width, but

this is not the case. The widths are extremely small and thus classify the sample as soft (i.e.

easily magnetized in the opposite direction). Also, the width of the 3 °K loop is larger than that

of the 70 °K loop. This suggests that the system is FM. As the thermal energy decreases the

atomic moments become harder to orient in the opposite direction, thus a higher coercivity.

Finally, as indicated most strongly by the 70 °K loop, the magnetization does not seem to be

significantly constant at the highest fields (70k Oe = 7 Tesla). This is likely because the system

is a *disordered* ferromagnet. This disorder could exist in a sample with a relatively low

percentage of manganese. Low concentrations lead to random intercalation of manganese into

the tantalum-disulfide layers. Since randomness does not ensure that each atomic moment, or

group of atomic moments, will have a nearest neighbor to interact with, it is possible that some

moments would remain misaligned. This seems reasonable when considering our sample to have
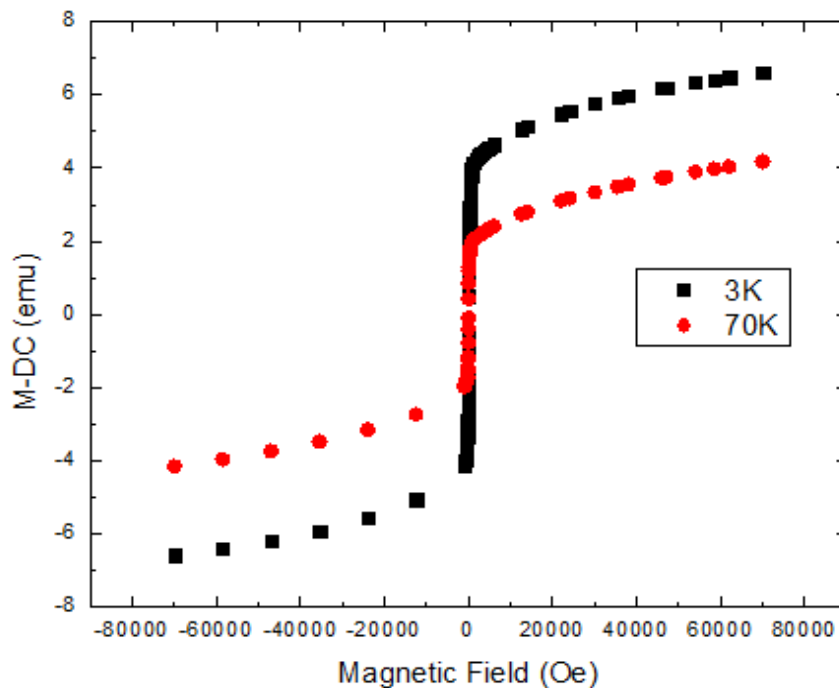
a concentration of 18% by EDX.

Figure 7. Two hysteresis loops for two separate

The final, and most complex, analysis techniques used on the nanostructured 18% sample
were the Arrott-Noakes and Kouvel-Fisher methods for extracting both critical exponents and
temperatures. The data sets required for these analysis techniques are relatively large compared
to the others employed. Magnetization and field data are taken at temperatures within an interval
containing the suspected critical temperature. The data are then manipulated to take the form of
$M^{1/\beta}$ and $\left(\frac{H_{int}}{M}\right)^{1/\gamma}$. Data in this form makes the Arrott-Noakes equation of state linear in its
terms if the exponents are correct. Plotting this data results in parallel lines, especially in the high
field regime. Figure 9 is a plot of the data taken using the second nanostructured 18% sample.
The values of the exponents are those that produce the straightest and most parallel set of lines.
In this case it is found that $\beta \approx 0.73$ $\gamma \approx 1.33$. The critical temperature is the isotherm (not
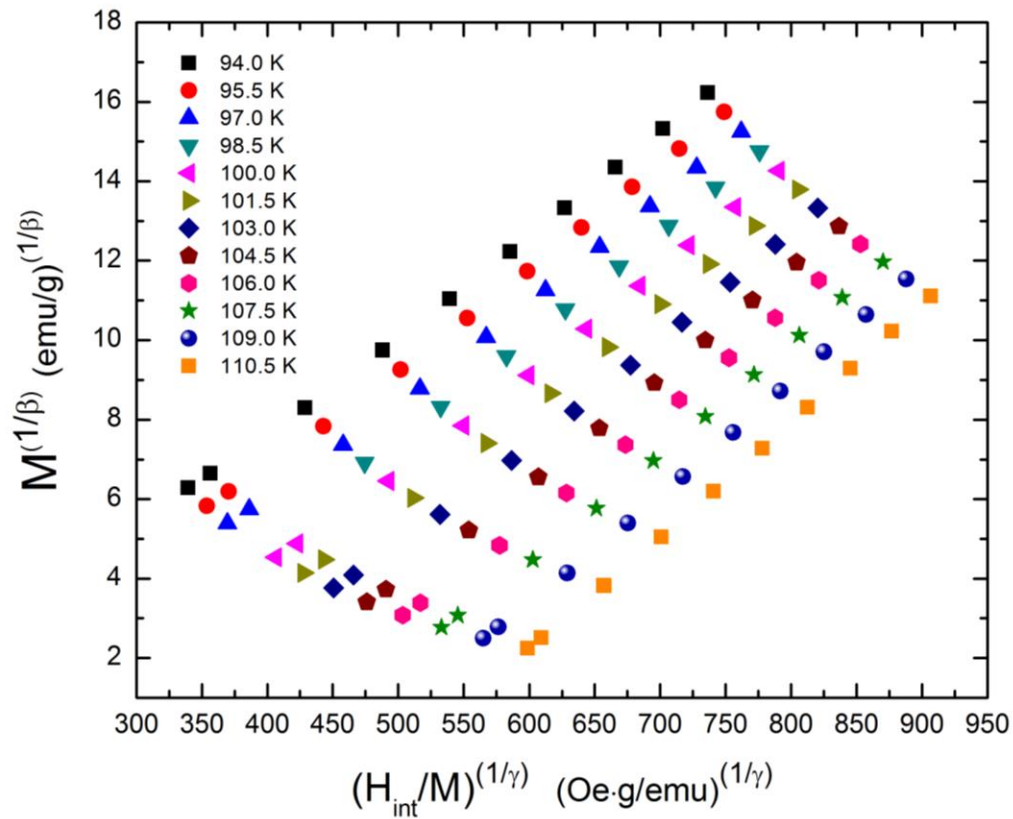

Figure 9. Magnetization and field data represented using the Arrott-Noakes
equation of state.

necessarily represented by data) that would have a y-intercept of zero. This is determined using

the Kouvel-Fisher method.

The Kouvel-Fisher method uses the critical exponents from the Arrott-Noakes method to

find the critical temperature. The data are manipulated into $M_0 \left(\frac{dM_0}{dT}\right)^{-1}$ and $\mathcal{X}_0^{-1} \left(\frac{d\mathcal{X}_0^{-1}}{dT}\right)^{-1}$ using

linear fits in Origin 8. As discussed in the Theories section, these two expressions are linear

functions of temperature with critical exponents as slopes and constants including the critical

temperature for intercepts. Figure 10 includes both sets of data in a single figure. Each of these

lines gives a different value of the critical temperature. These are compared in Table 3.

From this method, we have attained a precise value of the critical temperature.
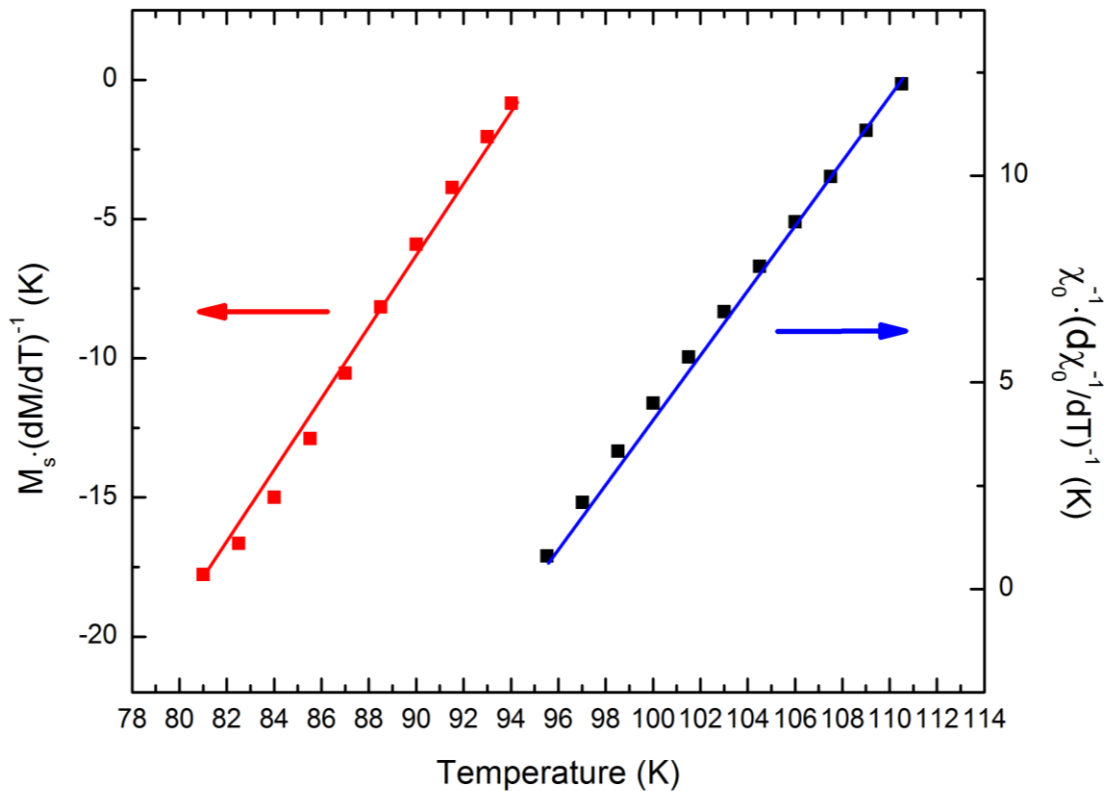

Figure 10. Kouvel-Fisher data for the nanostructured 18% sample.

Critical temperature from spontaneous magnetization	Critical temperature from zero-field susceptibility	Average
95 ± 2 K	94.1 ± 0.9 K	94 ± 1 K

Table 3. Values of the critical temperature of the nanostructure 18% sample calculated using the Kouvel-Fisher method.

As was discussed in the methods sections, a computerized version of the Arrott-Noakes and Kouvel-Fisher calculations was used. This program, written in *MatLab*, completed the Arrott-Noakes calculations by testing the linearity of the isotherms for various values of gamma and beta. Once the best values were calculated in this manner, the results were used for the Kouvel-Fisher analysis. Both methods would produce values for the critical temperature and exponents. Upon comparison, none of the values coincided extremely well. The disagreement between the critical temperatures may be due to uncertainties in the experimental data.

Crystalline Mn$_{0.25}$TaS$_2$

The mass of the sample was measured as before and is given in Table 4. As before, critical temperature was estimated using the Curie-Weiss method. This is shown in Figure 11. The parameters taken from the data fit are recorded in Table 5.

Mass of filled sample holder (grams)	Mass of empty sample holder (grams)	Mass of sample (grams)
0.8675	0.7046	0.1629 ± 0.0003

Table 4. Mass of the crystalline 25% sample.

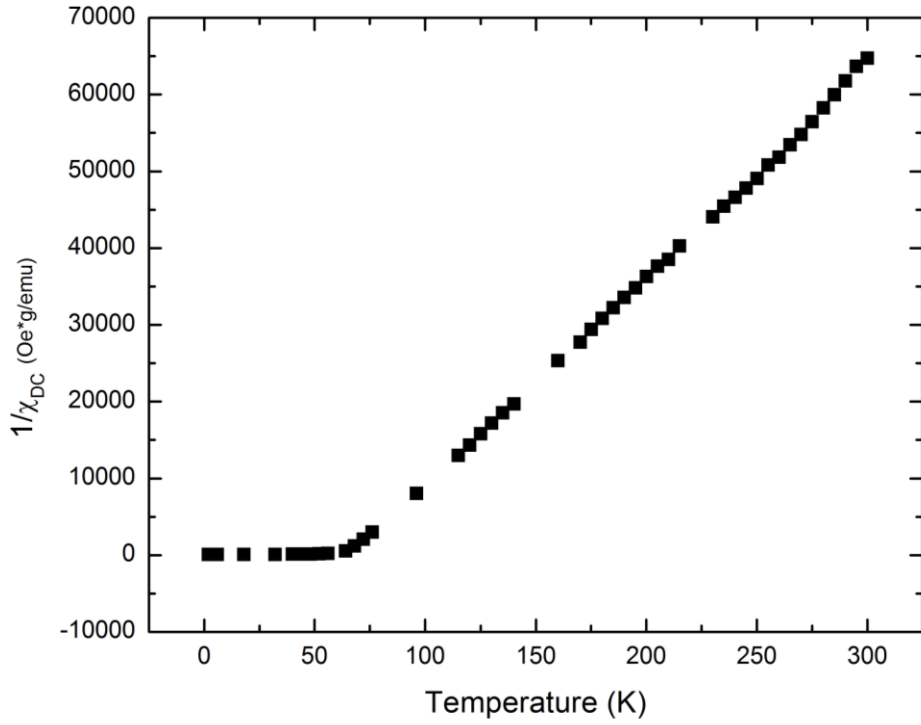| Fit Parameter	Value
θ (K)	66 ± 1
C ($emu \cdot K / Oe \cdot g$)	0.00368 ± 0.00002

Table 5. Curie-Weiss parameters.

Figure 11. A plot of the inverse susceptibility for the crystalline 25% sample. The purely paramagnetic regime begins at approximately 60
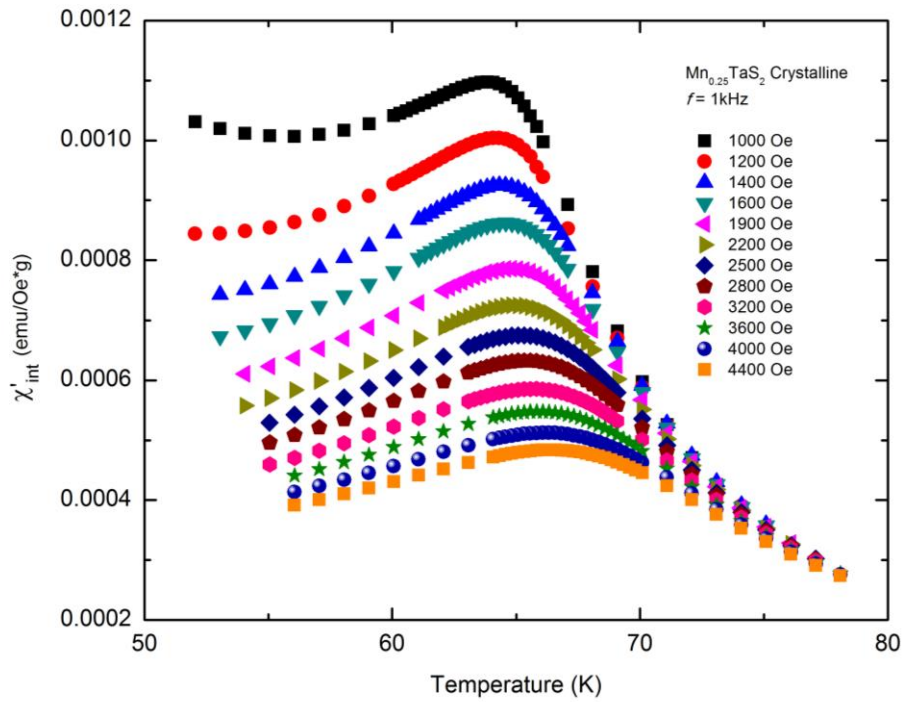

Figure 12. A plot of χ'_{int} as a function of Temperature. The shift in the peak as the applied field increases is a signature of a PM to FM transformation.

Again, the AC susceptibility data was plotted for various bias fields (Figure 12). The peaks in $\mathcal{X}'_{int}$ shift toward higher temperatures as the applied field is increased in strength. This is indicative of a ferromagnetic phase transition.

A scaling plot was created to better determine the transition temperature from the AC data. This is shown in Figure 13. In addition to the scaling plot is the inserted gamma plot. It is possible to extract the value for the critical exponent gamma using the same set of data as in the scaling graph.
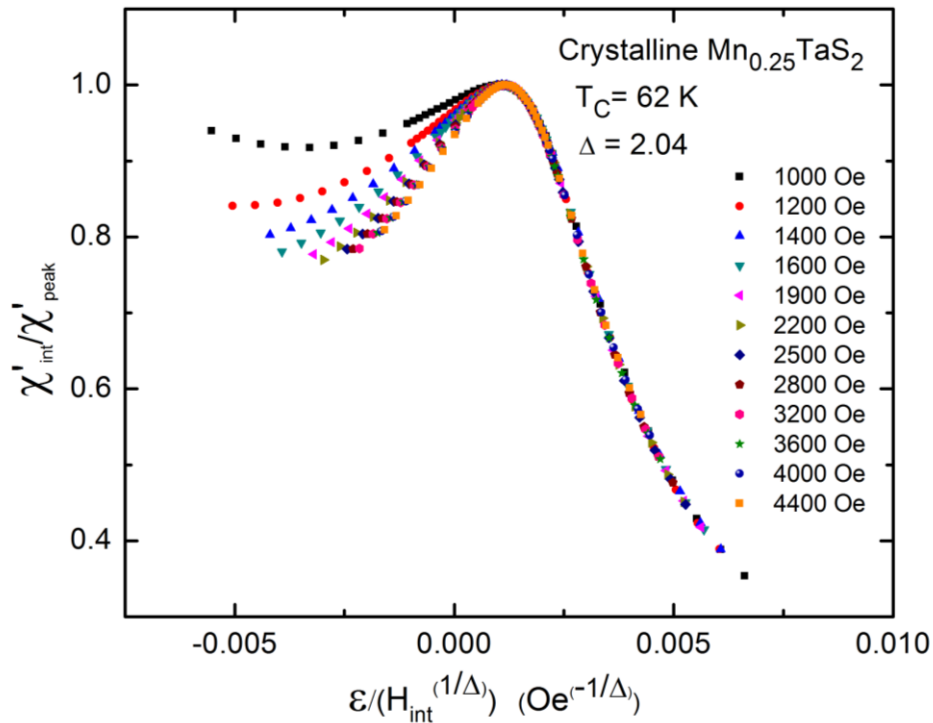

Figure 13. A scaling relation plotted in Origin 8. Such a relation utilizes critical exponents to show a universal curve or relation.
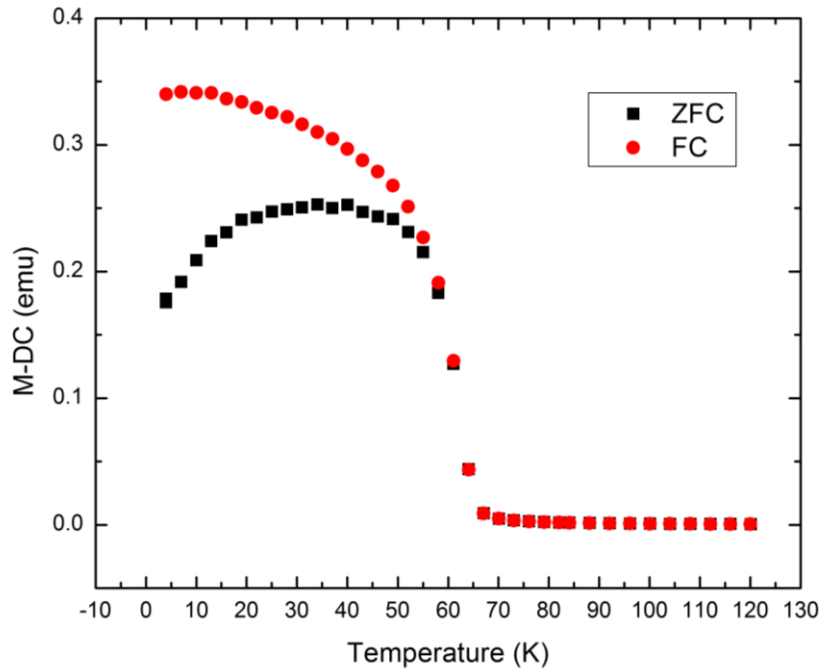
Figure 14. Plot of ZFC and FC data. The apparent position of the bifurcation comports with the believed PM to FM transition.
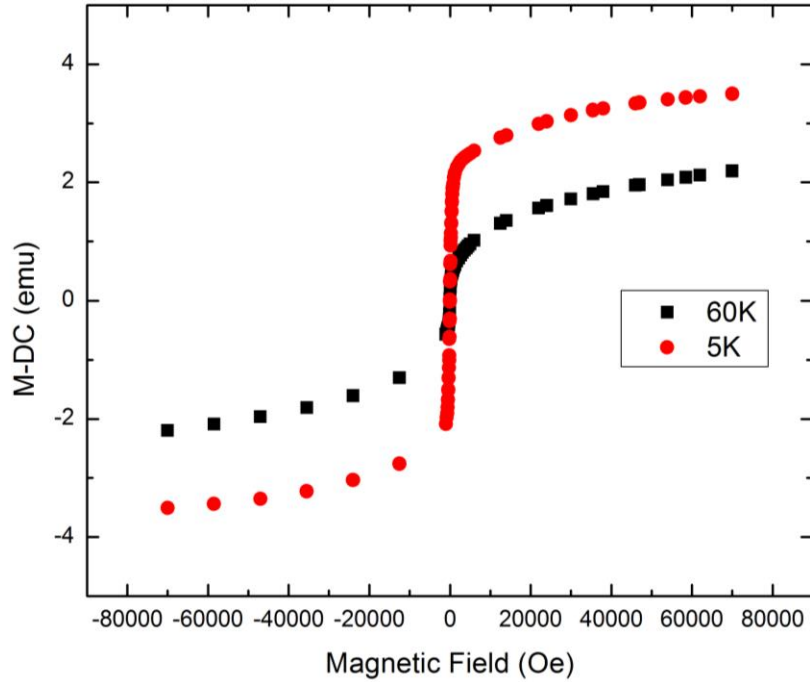

Figure 15. Two hysteresis loops for two separate

Zero-field cooled and field-cooled data were taken as before. The bifurcation, now at a

much lower temperature, is shown in Figure 14.

Next, the magnetic hysteresis of the sample was explored at 5 K and 60 K. As for the

previous sample, the loops are extremely thin.

The final analysis to determine the critical temperature of the crystalline sample was to

use both Arrott-Noakes and Kouvel-Fisher methods as before. Since the sample was crystalline

these methods worked exceptionally well. This can be seen in Figures 16 and 17. The lines

produced by the Kouvel Fisher data agree remarkably well on the transition temperature and

have a slope of nearly unity. Table 6 has the recorded temperatures as before. This temperature

fits within the intervals given by the previous methods. Before entering into a discussion of

these results, the data from several other nanostructured samples will be highlighted.
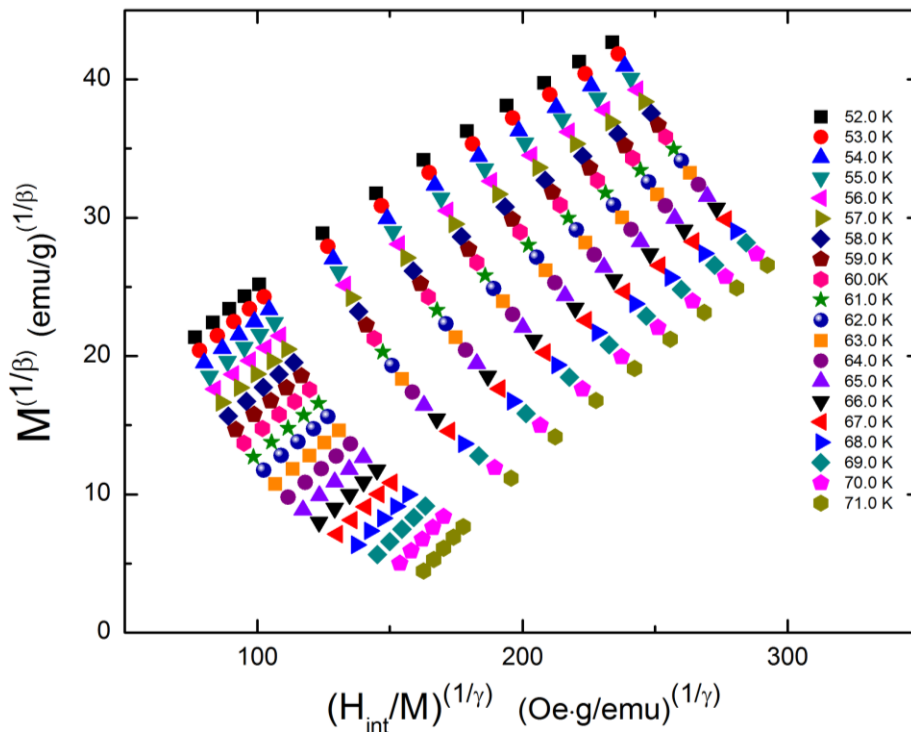

Figure 16. Magnetization and field data represented using the Arrott-
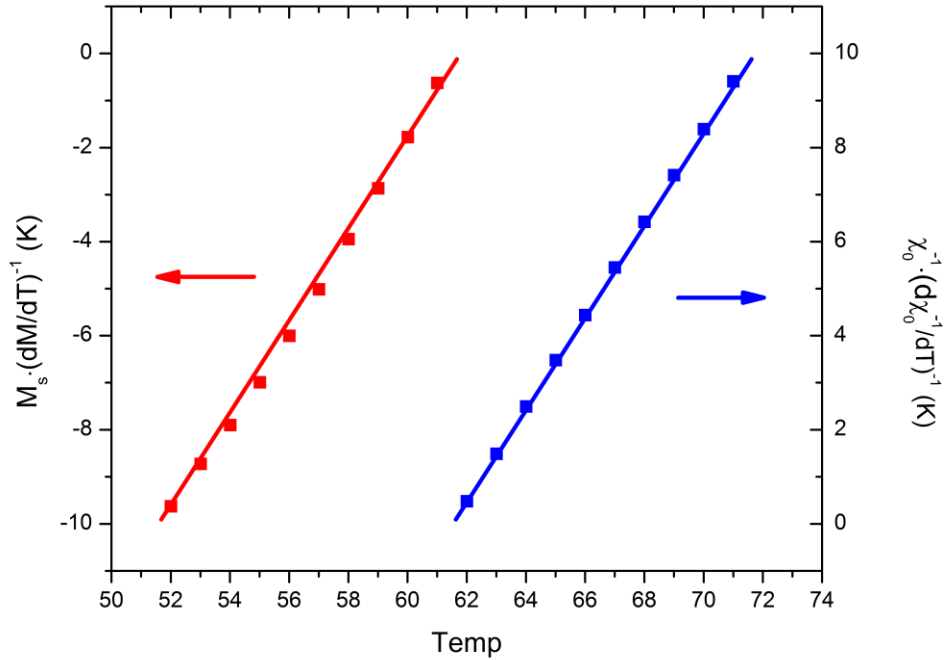Noakes equation of state. This data is for the crystalline 25% sample.

Figure 17. Kouvel-Fisher data for the crystalline 25% sample.

Critical temperature from spontaneous magnetization	Critical temperature from zero-field susceptibility	Average
62 ± 1 K	61.5 ± 0.1 K	61 ± 1 K

Table 6. Values of the critical temperature of the crystalline 25% sample calculated using the Kouvel-Fisher method.

Nanostructured Phase Diagram

The methods described above have been applied to nanostructured samples with concentrations of manganese ranging from 15% to 24%. The results are documented in the following phase diagram, Figure 18. Recall that the error of EDX analysis is ±10%.
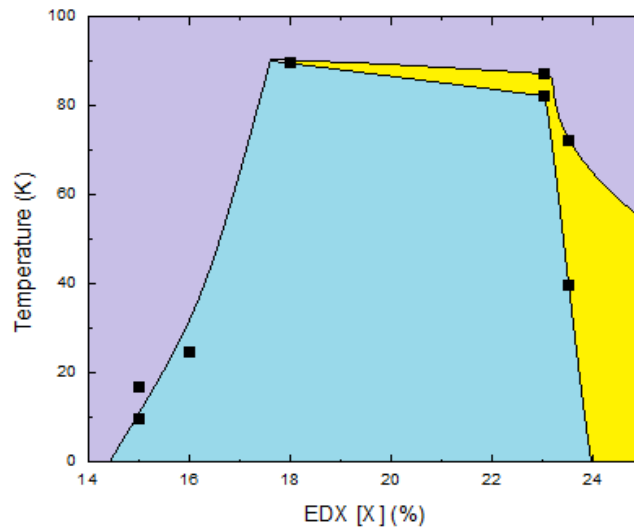
Figure 18. The culmination of data analysis completed on 6 samples. Blue represents the cluster glass phase. Yellow represents the ferromagnetic phase. Purple represents the paramagnetic phase. *Final image courtesy of Mathew Fleming, Physics Dept. University of Northern Iowa.*

Discussion and Conclusion

This project aimed to determine the characteristics of the magnetic phases of nanostructured and crystalline Mn_xTaS_2. To complete this task several analysis techniques were applied to data measured using a PPMS. The magnetic phase and critical temperatures of the nanostructured 18% and the crystalline 25% samples were described above.

To reiterate, the nanostructured sample was determined to have a transition from a state of paramagnetism to a state of ferromagnetism at $94 \pm 1\ K$ upon cooling. However, the critical exponents found when scaling the data were anomalously large ($\Delta = 4.45$), which may be the result of a second magnetic transition from a ferromagnetic state to a cluster glass state. In addition, the sample's hysteresis loop indicated that it was a soft, disordered ferromagnet.

The crystalline sample was determined to have a transition from a state of paramagnetism to a state of ferromagnetism at $61 \pm 1\,K$ upon cooling. The critical exponents of the crystalline 25% sample were comparable to those of basic theory ($\Delta = 2.04$).

The properties of the crystalline and nanostructured material could then be compared using the data produced by this project and the data from projects preceding this one. Results from previous projects indicated similarly anomalous values for the critical exponents of nanostructured Mn_xTaS_2. These values were reliably determined from scaling as in Figure 7 and 13. Anomalous exponents are indicative of the existence of a multicritical point in the phase diagram of non-magnetic systems. This may be the case for the nanostructured form of the material. More concentrations must be studied to create a more accurate phase diagram.

In addition to the anomalous exponents, it was possible to compare the critical temperatures of the nanostructured and crystalline forms of the material. The critical temperature of the crystalline form was known decrease with decreasing concentration. It follows then that the nanostructured form will have a higher critical temperature for the regions below x=0.25. The difference in critical temperatures may be due to differing geometry between the two forms. This could lead to stronger interactions between neighboring manganese atoms. Dr. Michael Roth, professor of physics at the Northern Kentucky University, has been studying the same nanostructured material using computational methods. His work will clarify the higher critical temperatures in the nanostructured materials.

The characteristics of both the nanostructured and crystalline forms of Mn_xTaS_2 have been studied at temperatures between $3\,K$ and $300\,K$ using a PPMS and several data analysis techniques. The specific critical temperatures and exponents were calculated and used to discuss the behavior of the material in regimes of concentration yet to be tested.

These results allow us to categorize the material as being ferromagnetic for low temperature intervals. The observed increase in critical temperature for the nanostructured samples provides support for a further investigation of magnetic, nanostructured two-dimensional materials.

Acknowledgements

References

Ajayan, P., Kim, P., Banerjee, K. (2016, September). Two-dimensional van der Waals materials. *Physics Today*, 69, 39-44.

Arrott, A., & Noakes, J. (1967). Approximate equation of state for nickel near its critical temperature. *Physical Review Letters, 19(14),* 786-789.

Fischer, S. F., Kaul, S. N., & Kronmuller, H. (2002). Critical magnetic properties of disordered polycrystalline $Cr_{75}Fe_{25}$ and $Cr_{70}Fe_{30}$ alloys. *Physical Review B, 65(1)*, 1-12.

Friend, R. H., & Yoffe, A. (1987). Electronic properties of intercalation complexes of the transition metal dichalcogenides. *Advances in Physics, 36(1),* 1-94.

Ginting, D., Nanto, D., Denny, Y. R., Tarigan, K., Hadi, S., Ihsan, M., & Rhyee, J. (2015). Second order magnetic phase transition and scaling analysis in iron doped manganite $La_{0.7}Ca_{0.3}Mn_{1-x}Fe_xO_3$ compounds. *Journal of Magnetism and Magnetic Materials, 395(1),* 41-47.

Hurd, C. M. (1982). Varieties of magnetic order in solids. *Contemporary Physics, 23(5),* 469-493.

Kidd, T. E., O'Shea, A., Griffith, Z., Leslie, S., Shand, P. M., Boyle, K. R., & Strauss, L. H. (2012). Synthesis of magnetic 1D dichalcogenide nanostructures. *Journal of Nanoparticle Research, 14:903,* 1-10.

Kouvel, J. S., & Fisher, M. E. (1964). Detailed magnetic behavior of nickel near its curie point. *Physical Review, 136(6A),* 1626-1632.

Peles, Arura (1999). Field-dependent magnetic and transport properties and anisotropic magnetoresistance in ceramic $La_{0.67}Pb_{0.33}MnO_3$. University of Manitoba Master's Thesis.

Shand, P. M., Cooling, C., Mellinger, C., Danker, J.J., Kidd, T. E., Boyle, K. R., & Strauss, L.H.

(2015). Magnetic states in nanostructured manganese-intercalated TaS$_2$. *Journal of*

Magnetism and Magnetic Materials, 382, 49-57.

Shtrikman, S., & Wohlfarth, E. P. (1981). The theory of the vogel-fulcher law of spin glasses.

Physics Letters A, 85(8-9), 467-470.

Stanley, H. (1971). *Introduction to phase transitions and critical phenomena.* New York, NY:

Oxford University Press.